Study of Ultranarrow Superconducting NbN Nanowires and Nanowires under Strong Magnetic Field for Photon Detection

By

Charles H. Herder III

Submitted to the Department of Physics in partial fulfillment of the Requirements for the Degree of

BACHELOR OF SCIENCE

at the

MASSACHUSETTS INSTITUTE OF TECHNOLOGY

[JUNE]
May, 2009

Signature of Author _____ 5-15-09
Department of Physics
(Date of Signature)

Certified by _____
Thesis Supervisor, Department of Electrical Engineering

Accepted By _____
Professor David E. Pritchard
Senior Thesis Coordinator, Department of Physics

Contents

1 Introduction

Photon detection is an integral part of experimental physics, high-speed communication, as well as many other high-tech disciplines. In the realm of communication, unmanned spacecraft are travelling extreme distances, and ground stations need more and more sensitive and selective detectors to maintain a reasonable data rate.[1] In the realm of computing, some of the most promising new forms of quantum computing require consistent and efficient optical detection of single entangled photons.[2] Due to projects like these, demands are increasing for ever more efficient detectors with higher count rates.

The Superconducting Nanowire Single-Photon Detector (SNSPD) is one of the most promising new technologies in this field, being capable of counting photons as faster than 100MHz and with efficiencies around 50%.[3] Currently, the leading competition is from the geiger-mode avalanche photodiode, which is capable of ~20-70% efficiency at a ~5MHz count rate depending on photon energy.

In spite of this, the SNSPD is still a brand-new technology with many potential avenues unexplored. Therefore, it is still possible that we can achieve even better efficiencies and count rates to keep up with the requirements of burgeoning technologies.

This photon detector consists of a meandering superconducting nanowire biased close to its critical current. In this regime, a single incident photon can cause a section of the detector to switch to normal conduction, producing a voltage pulse due to its now-finite resistance. An electron micrograph is given in figure 1.

The intrinsic limitations of the detector (disregarding the optical coupling mechanism and the support electronics) are dominated by two primary points. First is the efficiency with which the detector converts an absorbed photon into a voltage pulse. This is controlled by the behavior of the excited electrons at the point of incidence.[5] I will discuss this in greater detail in the next section.

The second is the electrothermal time constant of the detector.[13][14] This limits the relaxation time of the detector and therefore limits the maximum rate at which the detector can count photons.

As we will see, detection efficiency increases as the number of Cooper pairs that need to be excited into the normal state to switch conduction modes decreases. One way to decrease the bandgap is to decrease the cross-section of the wire. This has already been shown to increase detection efficiency, but this cannot be done to arbitrarily narrow wires. Not only is there a limitation to fabrication, but there are

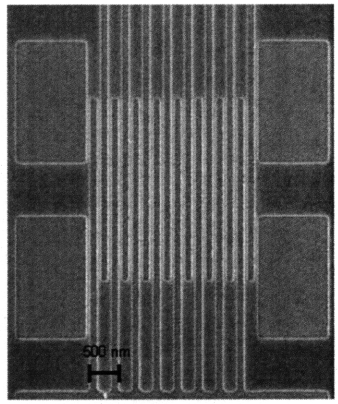

Figure 1: An electron micrograph of an example Superconducting Nanowire Single-Photon Detector (SNSPD). Current flows through the meanders in the middle from pads on either side. The wires in the meander are approximately 100 nm wide. Note that the additional formations exist to balance the dose between the edges and the middle of the detector.

also interesting quantum effects that occur at very narrow wire widths. Note that much of the research that has been done to understand these quantum effects has been undertaken on wires much wider than those we will be using. Simultaneously, most of the materials used previously have coherence lengths much longer than NbN. Therefore, even though our wires are narrower by a substantial factor, they are still wider than the coherence length of NbN. As such the validity of the one-dimensional approximation to be presented in in 2.2 is debatable for our wires. However, it should be apparent that regardless of behavior, thermal and quantum phase slips will be one of the limiting factors in producing ultra-narrow nanowire photon detectors.

Until now, photon detectors have only used current biasing techniques. However, it is well known that both magnetic field and current have the effect of reducing the energy required to excite superconducting charge carriers. Therefore, it may be possible to detect photons using magnetic field close to H_c instead of current close to I_c. It is important to note, however, that the readout of the detector in its current configuration depends on some bias current to produce a voltage pulse. Therefore, with the current detector architecture, one still needs a significant bias current.

For my thesis, I have first investigated the theory of supercurrents in ultranarrow wires and confirmed the behavior of this theory with our materials and fabrication techniques in order to establish a lower bound for wire width where photon detection

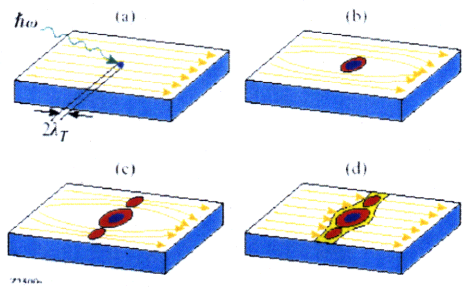

Figure 2: This is a schematic of how an incident photon produces a voltage pulse at the output. At (a), an incident photon is absorbed to produce an initial hot-spot shown in (b). The diverted supercurrent exceeds the critical current in the now-constricted wire in (c). Finally, a small section of the wire becomes fully resistive in (d), producing a voltage pulse.[18]

is still possible.

In addition, I have constructed and executed an initial experiment to test how photon detectors behave under magnetic field bias conditions. I have measured how these different bias conditions affect the efficiency of the detector as well as the dark count rate.

2 Theory of Photon Detection

The theory for photon detection in current-carrying nanowires is a topic of some debate, although many features are now well established.[5][18] Effectively, an incoming photon will break cooper pairs locally in a nanowire, causing a local "hotspot" that has normal resistance. With a bias current close to the critical current, this will cause that section of the wire to go normal, and Joule heating will subsequently expand the nanowire hotspot. One then sees a voltage pulse across the detector.

2.1 Hotspot Theory

When a section of the detector goes normal due to an incoming photon, the effective resistance of the detector increases dramatically, and therefore the current though the detector drops temporarily.

Now, two things happen simultaneously. First, the heat localized in the hotspot

must diffuse to other parts of the detector or substrate. Second, the detector is inductive, so there is an L/R relaxation time of current returning to the detector.

However, these are competing processes. Any current through the detector will end up in joule heating of the resistive section of the detector, extending the amount of time it takes to cool the hotspot back down. If the L/R time constant is some fraction longer than the thermal time constant, then the system properly resets into a superconductive state. Otherwise, the detector latches into a normal state, since a self-maintaining hotspot is a stable solution.[13][14]

These two time constants determine the output pulse size and therefore the maximum count rate of the detector.

2.2 Dark Counts

Dark counts, simply put, are spontaneous counts generated by the SNSPD without the presence of a photon. They can be explained by the generation of phase-slip-centers PSC's that cause a 2π fluctuation in the order parameter. This in turn generates a pseudo-hotspot that produces a voltage pulse identical to those produced by photons. [6]

Gol'tsmann et al. have done significant inquiry into the origin of these dark counts and found that they correlate strongly with the LAMH theory of phase slips, both for thermally activated as well as quantum. The dependence for this model is given by:[17]

$$R_{dc} = R_0 \sinh\left(\frac{I_b}{I_0}\right) \approx R_0 e^{\frac{I_b}{I_0}} \tag{1}$$

The above approximation is valid in the limit of large I_b. R_{dc} is the dark count rate for an bias current I_b. I_0 is a characteristic cutoff current for dark counts that is material and geometry-dependent, but is always some fraction of I_c. The multiplicative term R_0 is a complicated expression derived from the tunnelling rate through the energy barrier ΔF_0, where:

$$\Delta F_0 = \frac{8\sqrt{2}}{3}\frac{H_c^2}{8\pi}A\xi \tag{2}$$

In the above, H_c is the critical field, ξ is the Ginzburg-Landau coherence length, and A is the cross-sectional area. Therefore, for thermally activated slips, we can characterize the probability of overcoming this barrier by an attempt rate Ω multi-

plied by the exponent of the barrier divided by the thermal energy. This has been experimentally confirmed, yielding:

$$R_0 = \Omega \times \exp\left(\frac{-\Delta F_0}{kT}\right) = \frac{L}{\xi}\frac{1}{\tau_s}\left(\frac{\Delta F_0}{kT}\right)^{\frac{1}{2}} \exp\left(\frac{-\Delta F_0}{kT}\right) \tag{3}$$

In this case, we are using the temperature-dependent attempt frequency for Ω calculated by McCumber and Halperin.[11]

An important thing of note is that the dark count rate is proportional to the number of potential PSC's on a device and how they are distributed along the wire. On a highly nonuniform device with a dominant constriction, there may be only a few PSC's localized around this constriction. On the other hand, a highly uniform device can have a great deal more PSC's spread throughout the device. However, for photon detection to be efficient, one also needs PSC's to be distributed along the wire (i.e. no constrictions) to ensure that the incoming photon actually switches the device. Therefore, it seems apparent and has been experimentally verified that Quantum Efficiency (QE) increases as the dark count rate increases.[5][17]

2.3 Quantum Phase Slips

The dark counts mentioned above are due to thermal excitations over the energy barrier ΔF_0 between adjacent supercurrent states. Effectively, it can be observed as a loss of 2π in the order parameter at some singular point.[7]

Now, in the case above, we are observing Johnson noise, and this purely thermal excitation allows us to surmount the energy barrier. Now, recalling equation 2, we observe that the energy barrier is proportional to the cross-sectional area of the wire.

In theory, if we make this energy barrier small enough, we should be able to observe quantum tunnelling through it. This turns out to be exactly the case. However, due to the intrinsic energy associated with nonzero loop current, adjacent states do not have the same energy. Therefore, the energy profile becomes a washboard potential.[9]

The tunnelling rate through this profile has already been solved to have the dependence on the energy barrier.

$$R_{qps} = \Omega' \times \exp\left(\frac{-\Delta F_0}{\hbar/\tau_s}\right) \tag{4}$$

Where, Ω' is the repetition rate and τ_s is the Ginzburg-Landau time constant of the system:

$$\tau_s = \frac{\pi\hbar}{8k(T_c - T)} \tag{5}$$

This is extraordinarily reminiscent of the thermally activated dark counts studied above. The only difference is the dropoff rate: kT is now replaced by $\hbar/\tau_s$. If one re-derives the attempt frequency by McCumber and Halperin, the same replacement occurs.[11] Therefore, the dark count rate due to quantum phase slips has the *exact* same dependence as described in equation 3 with the thermal energy replaced by the characteristic quantum energy.

Even though the dependence is the same, this replacement dramatically affects the dropoff rate with temperature. As a result, we can observe very significant phase slip rates even at temperatures substantially below T_c with negligible applied current. This could potentially cause a problem for photon detectors with exceedingly narrow wire widths. It is the objective of my experiment to characterize this behavior.

The above physical description is the simplest model for quantum phase slips. As the geometry and material properties change, it is not guaranteed that the model accurately reflect the behavior of the system. For example, some superconducting nanowires investigated by Bollinger et. al. never reach the superconducting state at any temperature.[8] In addition, our wires are not truly 1-dimensional. The above calculations assume the order parameter varies only in one, but our wire widths are about twice as wide as the coherence length. Therefore, the idea of phase slip centers may not even be applicable to our geometry. This must be tested empirically.

These phase slips described above are due to a completely independent physical phenomenon from thermal phase slips and as a result are completely uncorrelated and therefore additive. Thermal phase slips have a much higher overall rate, so quantum phase slips are generally unobservable until lower temperatures when thermal phase slips have been suppressed.

Finally, like thermally activated phase slips, these slips are heavily dependent on the distribution of PSC's along the wire. Quantum phase slips have an identical dependence on ΔF_0, so this is not surprising.

2.4 Potential Advantages of Ultranarrow Superconducting Nanowires

Ultimately, the SNSPD depends on reducing the energy barrier ΔF_0 to a small enough value such that a single photon can surmount this barrier or tunnel through and a

render a small section of the detector as normal.

Recently, people have began to fabricate wires with widths down to 10nm.[10] As shown above, the energy barrier depends in part on the cross-sectional area of the wire, so one can also decrease ΔF_0 of the device by making it narrower. The first benefit of this is that the number of PSC's increases. This will increase detector efficiency as well as dark count rate.

In addition, the size of the hotspot increases relative to the overall width of the detector. This means that when the initial hotspot forms, the bias supercurrent must flow through a much smaller cross-sectional area, increasing the likelihood of exceeding the critical current and thereby producing a voltage pulse. Combining both of these effects results in a decrease in cutoff current for the photoresponse, and an increase in detection efficiency.

However, there are a number of potential complications in this regard. First, from the standpoint of fabrication, a narrow (10nm) wide wire is significantly more difficult to fabricate than a 100nm wide wire and therefore may not be as well behaved. In addition, with ultranarrow wires, one begins to see PSC's without significant bias current at liquid helium temperatures.[9] This is possibly because at this small cross-section, quantum phase slip centers become significant, and they have a much slower drop-off rate with temperature than thermal phase slips.

2.5 Potential Advantages of Magnetic Field Biasing

I am also investigating the option of suppressing ΔF_0 through magnetic field biasing. This could potentially increase the detection efficiency because it affects the energy barrier in a similar way to decreasing the wire width. As shown in equation 3, R_0 is dependent on H_c just as it is on A.

It is an important note that we are not changing the intrinsic H_c of the material, but by biasing the superconductor at nonzero H, we are decreasing the effective incremental magnetic field H_c' that can be applied before the superconductor changes to the normal state. Therefore, we are reducing ΔF_0, without changing any geometric or material properties. This should have the same effect as decreasing the cross-sectional area. It should increase the dark-count rate as well as detection efficiency.

In addition, during the switching process, joule heating occurs due to the bias current. With a smaller current on an equivalent sized detector, less energy will be dissipated, so the overall relaxation time should decrease. Therefore, one should be able to attain faster count rates by decreasing the L/R time constant further than

was previously attainable without latching.

Since magnetic field biasing has no effect on the actual geometry of the detector, it should not affect the ratio of the cutoff current of the detector to its critical current. Therefore, we must operate at approximately the same fraction of I_c to achieve reasonable efficiency. If we have increased the number of PSC's, one increases the number of dark counts as well as the efficiency.

Finally, another advantage of biasing with magnetic field is the the field is very uniform and very low noise. With current biasing, the current must pass through both constricted and wider sections of wire, meaning that the detection efficiency may decrease for certain sections of the detector. In addition, since we will be using a superconducting magnet with a persistent switch, there is negligible noise in the applied field, whereas a current bias will always have some output-referred source noise.

In spite of the potential benefits, both of the above methods have an added difficulty. While there are many things that can be gained by decreasing the bandgap, one also must contend with the fact that the readout pulse will decrease in size. At the scales we are looking at, the pulse is approaching the noise floor. As a result, there is only so far we can push either method, regardless of other engineering limitations.

3 Experimental Apparatus - Ultranarrow Wires

The experiment to test the behavior of NbN nanowires as width approaches zero was simpler to execute than the magnetic field experiment since we already had the test equipment capable of characterizing the detector.

3.1 Cryogenic Setup

I performed this experiment in the cryogenic probe station consisting of a liquid helium flow cryostat. The samples themselves were mounted on the cold head using silver paint on a copper base. Temperature probes were located inside the cold head and adjacent to the sample mount to ensure the samples reached the proper temperature. I made electrical contact with the samples using a micropositioned RF probe to land onto the sample pads. This is shown in figure 3.

The functionality of the above methodology has been well established due to numerous tests on this cryogenic platform. However, the primary difference in my

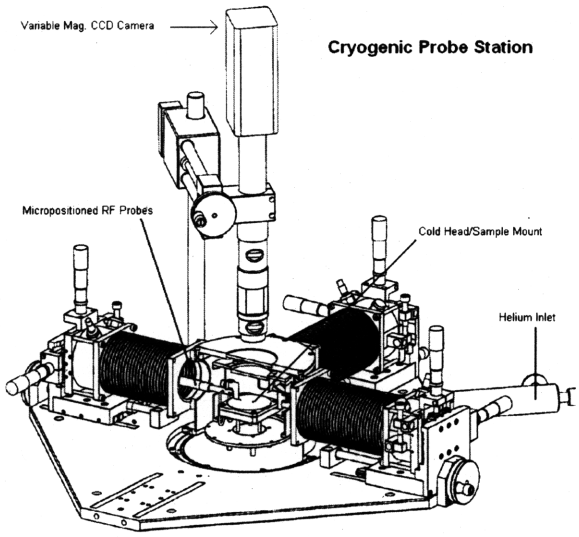

Figure 3: A figure of the cryogenic probe station used to characterize the properties of ultranarrow superconducting nanowires.

experiment lay in the supporting electronics.

The purpose of my experiment was not to count photons, but rather to characterize quantum phase slip rate in NbN, so I did not need any RF electronics. Rather, I simply wanted to characterize R versus T very accurately. Therefore, I used a precision parameter analyzer to trace these curves.

Since the entire system now is operating at DC, I used a bias tee as a low-pass filter to remove any high frequency noise introduced by the parameter analyzer.

To test that this setup was in fact performing as expected and not introducing too much noise on the detector, I measured the critical current both with the parameter analyzer and with our custom low-noise current source in an identical configuration and ensured that they were the same. Therefore, I can be confident that IV curves traced by the parameter analyzer are in fact due to intrinsic properties of the detector, rather than due to an overabundance of noise sourcing from the parameter analyzer.

I must also note that the relation between dark count rate and the resistance is through a simple proportionality constant. Each phase slip produces a voltage pulse. If we sum and average these pulses, we can approximate it as a DC voltage. This voltage is related as a hyperbolic sine on current, but for small changes in current, this is approximately linear, yielding an ohmic relationship:[9]

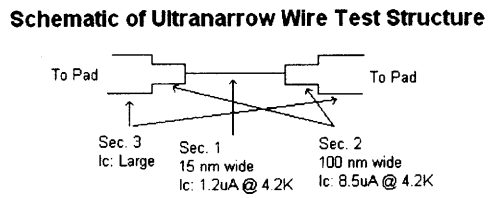

Figure 4: A schematic of the template used to fabricate the ultranarrow wires. Note that there are two bulkheads on either side use to connect the narrow wire to the pads. These two regions have indicated widths and I_c's. Section 2 became important as I took measurements near $T = T_c$, as it became resistive.

$$R_{mqt} = B\frac{\pi\hbar^2}{2e^2}\Omega' \exp\left(\frac{-\Delta F_0}{\hbar/\tau_s}\right) \tag{6}$$

Where B is an arbitrary scaling factor. Therefore, even though we are observing events that occur on a GHz frequency scale, we can characterize them approximately by observing only the DC components.

3.2 The Detector

The 'detector' in this case is just a single nanowire. Due to dose effects, we were able to achieve the most consistent yield with only a single short wire with no bends. Ultimately, I used a series of wires of varying widths between 15 and 25 nm. The wires themselves were 5 nm thick and 100 nm long. These devices were fabricated by Dr. Eric Dauler.

An important note for this is that the support structures connecting the wires to the pads are initially 100 nm wide and taper up to the size of the pad. This becomes important because it affects the overall resistance of the wire near the critical temperature. Therefore, it affected the behavior of the thermal phase slips.

4 Experimental Results - Ultranarrow Wires

Using the above experimental setup, I tested several devices with varying wire widths. I characterized only the DC bias current versus DC voltage. Although this signal

contains high frequency components, I can extract all of the necessary parameters from the DC component of the signal.

4.1 R vs. I_b

I characterized the I vs. V curves for several different nanowires at varying temperatures. I fit the these curves both below and above the critical current to obtain the resistance. I have fit one of the I/V curves with a hyperbolic sine to demonstrate the accuracy with which our data follows LAMH/QPS theory in the current domain. We can directly observe the linear behavior near zero current, which is indicative that our approximation that the count rate increases linearly with bias current is good in this region.

Using these values, I measured the resistance versus temperature. An example plot of one of these curves is given in figure 6.

Note that the resistance in fact has the expected dominating exponential dependence on temperature. In the plot above, I have shown resistance predictions from thermal (LAMH) and quantum (MQT) phase slips. Note that these are not fit lines. These are approximate model predictions given device parameters.

We do not have a good enough sequence of data at low temperatures to fully characterize the MQT model. However, it is readily apparent that the LAMH thermal phase slip model is inadequate in explaining these low-temperature points. Therefore there must be some additional contribution. Quantum phase slips explain this residual resistance, but we cannot confirm our theoretical model without additional data points.

Note also that I did not characterize the thermal phase slips above 10K, simply because our test structure made this impossible. As we approach the critical temperature, not only do we observe resistance due to phase slips from the 15 nm stretch of wire, we also observe phase slips on the thicker 100nm bulkhead. This is demonstrated by the fact that the resistance beyond the critical current of the 15nm wire changed from 8K to 15K between 4.2K and 10K (see figure 5). Although we are still below the suppressed I_c of section two (see figure 4), we are observing additional resistance due to the fact that this wire now has finite resistance due to phase slips since we are so close to T_c. Therefore, I have ignored these data in favor of simply observing resistive behavior in the region where I am sure I am only studying the ultranarrow wire itself.

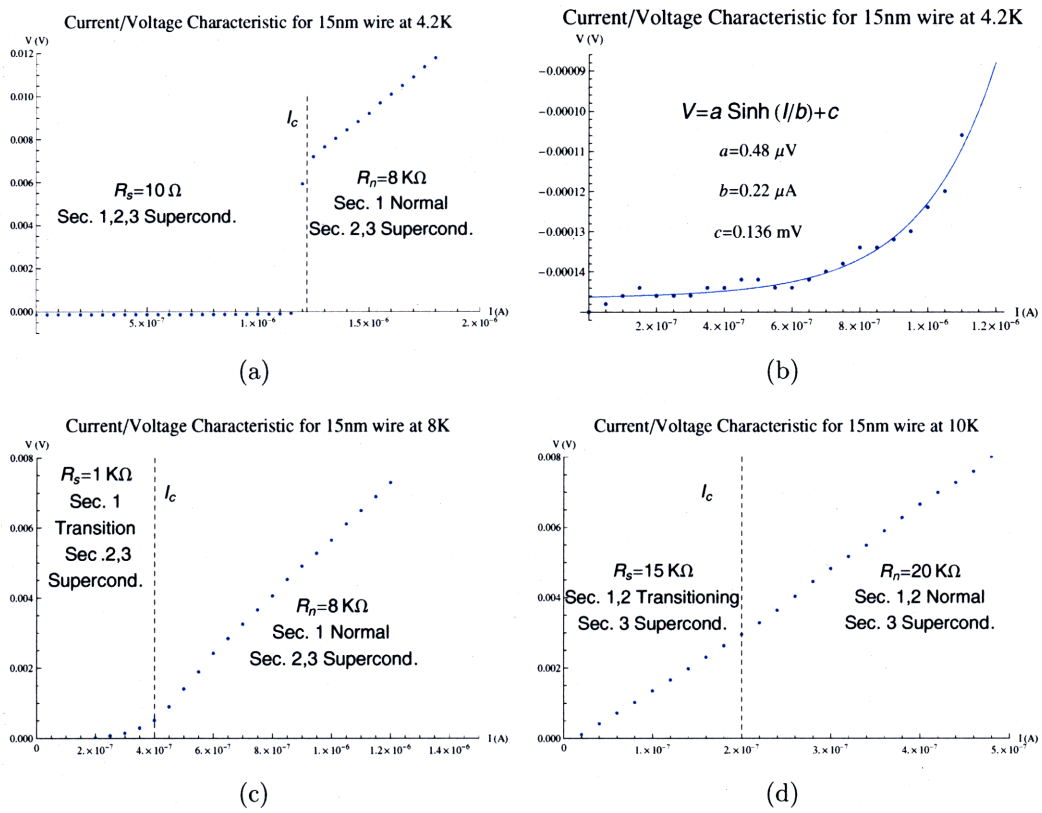

Figure 5: Plots of I vs. V curves for 15 nm nanowire at various temperatures. Note that the normal resistance is substantially higher for (c) at 10K. This is due to added resistance of the bulkhead. Also note that in regions far away from I_c, the resistance relationship is purely ohmic. This is demonstrated by (b), a zoomed in look at the superconducting resistance at 4.2K. Note the sinh(I) dependence that approaches linear for $I << I_c$

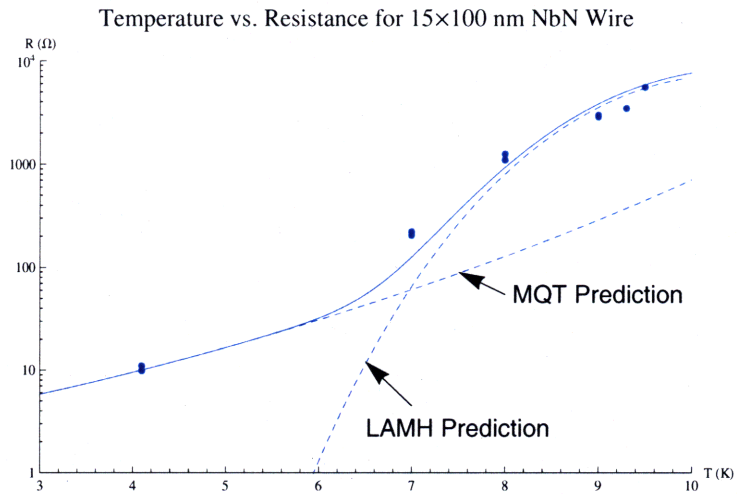

Figure 6: Plot of R vs. T for a 15 nm wide, 100 nm long, 5 nm thick nanowire. Note the expected dominant exponential dependence on temperature. LAMH phase slips (thermal phase slips) die off faster than exponential, so these cannot explain the low-temperature resistance. The MQT model adequately explains these data.

4.2 Discussion

The key thing of note is that there is still a significant resistance at liquid helium temperatures (10 Ω). Note that this is not residual resistance of my measurement, as I checked the internal resistance of the system by grounding the RF probe and measuring background resistance. This was on the order of 1Ω or below. This means that the count rate is significant enough to yield a measurable voltage and therefore is probably unsuitable for photon detection. To quantify this, we can make a rough estimate the count rate for a given voltage appearing across the detector.

Consider an individual pulse as 5 ns wide (an overestimate). I measured the normal resistance of the wire to be ~8 KΩ. The entire wire will not become resistive at a single switching event, so this is also an overestimate. With a bias current of 1 μA, each pulse contains 4×10^{-11}V s. To achieve a resistance measurement of 10Ω, we must measure a voltage of 10^{-5} V, which implies a count rate of over 250 KHz to have the proper mean voltage (compared to a standard photon count rate of 1MHz). Given that I have overestimated the coefficients, this means that 250KHz is a minimum count rate. To make things worse, since the resistance is ohmic even at low currents (the hyperbolic sine dependence on current is approximately linear for

small current), this count rate seems to be independent of bias current when using the above method.

This experiment has set a lower bound on the possible widths of nanowires for superconducting single-photon detectors. Given these data, it is not feasible to expect a 15 nm wide wire to be able to detect photons due to the large dark count rate. A possible initial solution to this is to operate at lower temperatures. However, this has a limit of approximately 2K without adding more special equipment.

At 4.2K, the minimum wire width appears to be between 20-30 nm before one becomes overwhelmed with phase slips. As mentioned above, this bound may be reduced to between 10-20 nm if one is operating at 2K, but this remains to be tested.

5 Experimental Apparatus - Magnetic Field

The second experiment I performed was to investigate the behavior of the detector under magnetic field bias conditions. Unlike the previous experiment, this experimental apparatus had to be constructed from the ground up before I could begin testing.

5.1 Cryogenic Setup

The cryogenic platform is constructed from a Janis 10CNDT liquid helium cryostat. This is an immersion style cryostat with a 10L capacity. Inside of the dewar, I constructed an outer probe that contains the magnet, fiber optics, power feedthroughs, and a protective sheath for the inner probe. The magnet itself is an American Magnetics NbTi solenoid style superconducting magnet rated to 65 kG at 45.2 A before quenching. The field is linearly dependent on current: 1.438 kG/Amp. I am using a refurbished Intermagnetics Model 150-M superconducting magnet power supply capable of delivering up to 150 A of current.

The inner probe consists simply of a rigid non-magnetic stainless SMA cable with a sample mounted on the end. This mount consists of an SMT SMA termination soldered to a PCB. The detector is attached on the other side with silver epoxy and wirebonded to the appropriate pads.

Some important notes are that the entire inner probe as well as the sample mount must be electrically isolated from the magnet and the dewar manifold. Even a weak electrical contact provides parasitic capacitance which prevents the detector from

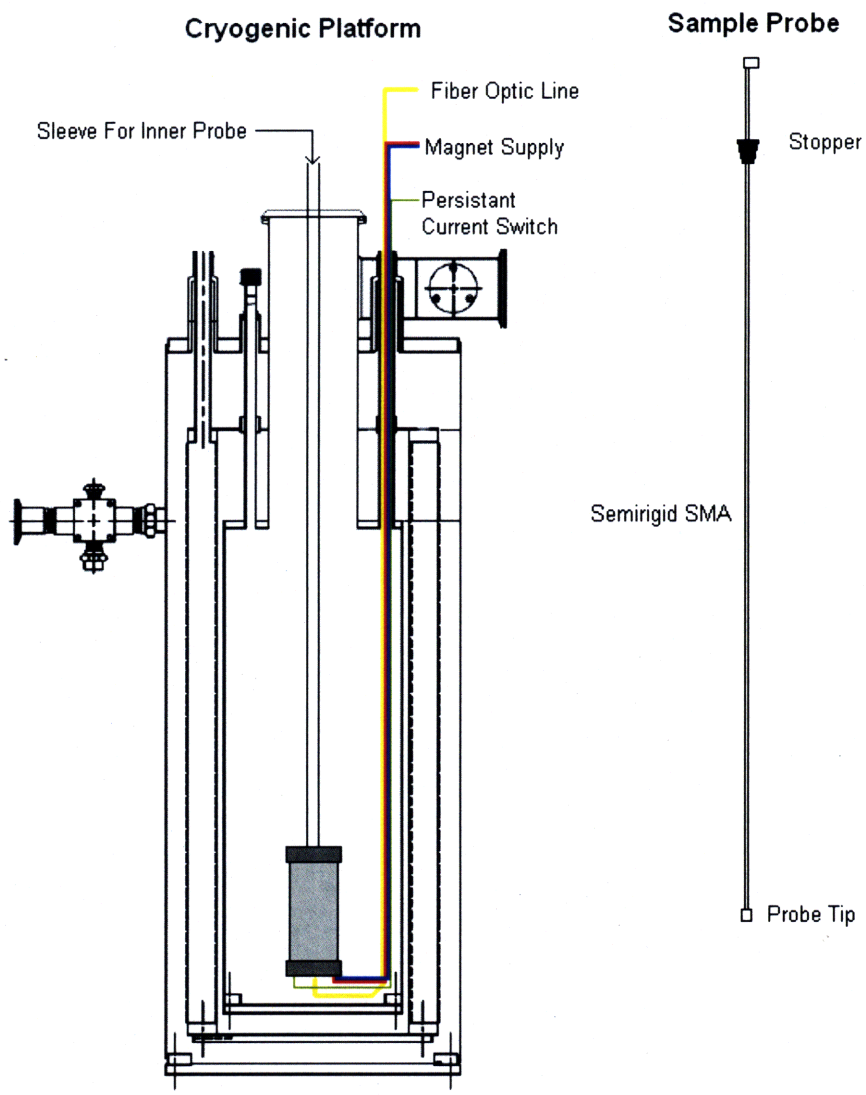

Figure 7: This is a schematic of the experimental apparatus I constructed. Note that the feedthroughs at the top of the dewar are all capable of low vacuum. This is necessary to be able to pump out the dewar before cooling. Also, the entire probe can be dynamically moved up or down to change the system's temperature if necessary.

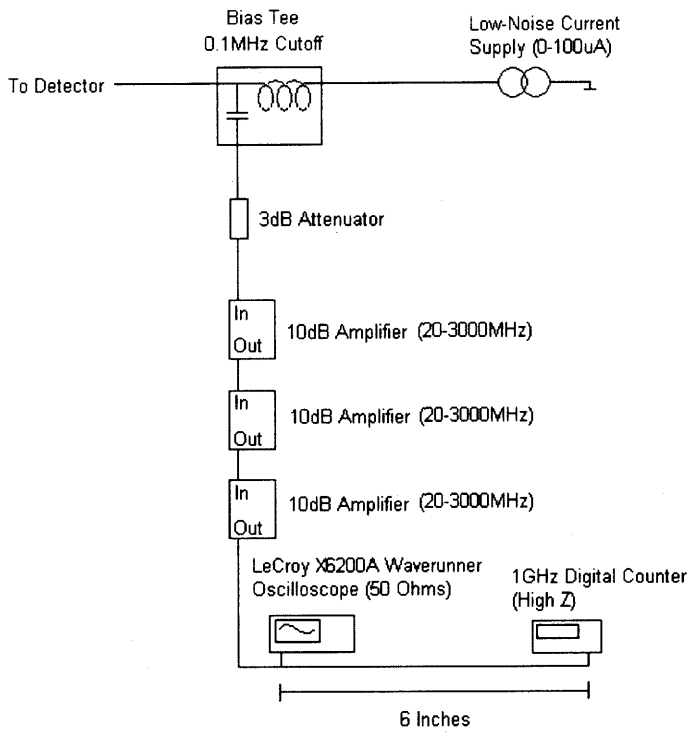

Figure 8: Above is a schematic of the RF electronics involved in this experiment. Due to the sensitive nature of this experiment, the entire setup is heavily shielded. Note that the discriminator/amplifier is high Z, but is located close to the oscilloscope's 50 Ohm termination, so reflections have been minimized.

functioning correctly.

The optical setup is exceedingly simple, consisting of a Thorlabs S1FC1550 1550nm fiber laser source operating at 0.7mW output. This laser then couples to the feedthrough fiber optic line with an unknown attenuation. Finally, the fiber remains unterminated and unfocused at the base of the magnet. This provides me with the ability to have consistent illumination across multiple bias conditions, but it is impossible to calculate absolute detector efficiencies with this setup. Therefore, all of my count rate data must be comparative.

5.2 RF Setup

The RF setup is fairly standard for SNSPD operation. The detector line enters into a Mini-Circuits 50 ohm bias tee with a low-noise current supply on one side and the RF amplification/detection circuitry on the other. The tee itself has a cutoff frequency at 0.1 MHz and a roll-off frequency at 4.2 GHz. For this experiment, we are using a pure DC bias through the inductor and the RF signal is ~1GHz, so there should be no leakage in either direction.

The low-noise supply is battery powered and is capable of delivering DC currents up to 100uA with a total output referred current noise no greater than 1-10nA. This supply is tied to the inductor of the bias tee to provide bias current for the detector.

The RF side consists simply of three Mini-Circuits 10dB RF amplifiers with active input frequency range between 20-3000MHz. Note that the additional 3dB attenuator seen in figure 8 exists solely to prevent oscillations between the amplifiers and the bias tee. The fully amplified signal is then passed to a LeCroy Waverunner 6200A (10Gs/s) and an HP 5316B universal discriminator/counter.

One important note is that the discriminator/counter has a high Z input, whereas the rest of the circuitry is all 50 Ω terminated. To compensate for this, I have located the discriminator very close (within 6 in.) of the 50 Ω termination of the oscilloscope. As a result, this prevents significant reflections on the transmission line. I have explicitly confirmed this by observing the pulse shape on the oscilloscope itself.

It is also not necessary to have 30dB of gain to observe voltage pulses at the output (20dB is usually enough). This additional gain is due to the fact that the discriminator/counter is significantly less sensitive than the oscilloscope, and therefore it needs the extra headroom. Additionally, this experiment reduces the effective critical current of the nanowire, and therefore the output signal is smaller than it is normally. Therefore the extra gain is helpful in this regard.

All of the components except the oscilloscope and the counter are located in a heavily shielded box. Each part is grounded to this box to minimize electromagnetic pickup. Even with these precautions, I still observed a measurable 100MHz electromagnetic pickup. This pickup is originating in the bias tee. I minimized this effect as best as I could by grounding and shielding this component, but the noise did not disappear entirely. The remaining connections are all made using shielded semi-rigid SMA coax cable.

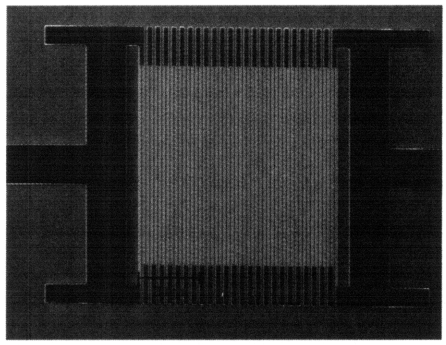

Figure 9: An SEM of the architecture of detector I used in this experiment. This SEM was taken from the same batch and has the same geometric specifications, but is of a different detector.

5.3 The Detector

All of our detectors are NbN deposited on Sapphire substrate. I am using a detector with ~6nm thick NbN, 100nm wide wires with a 200nm pitch. The active area of the device is 10μm $\times$ 10μm. The detector was fabricated by Dr. Eric Dauler. Although the entire batch is processed on a larger wafer, the wafer was diced to be 2mm by 2mm so that it could fit into the bore of the magnet. This sample was then bonded to a small PCB and the detector pads were wirebonded to the appropriate pads on the PCB (see figure 10).

I have built two probes to be mounted inside of the magnet: one with the detector parallel to the B field and one with the detector perpendicular. However, for this experiment I only used the mount with the detector perpendicular to the B field.

All of my experiments concerned a single detector mounted on the perpendicular mount. The detector has a measured critical current (at 4.2K with no magnetic field) of 19.3uA.

6 Experimental Results - Magnetic Field

6.1 Procedure

To maintain as clean of an environment as possible, I radiatively cooled the inner chamber of the cryostat by maintaining a constant level of liquid nitrogen in the outer shield. This takes approximately 4.5-5 hours. At this point, one fills the inner

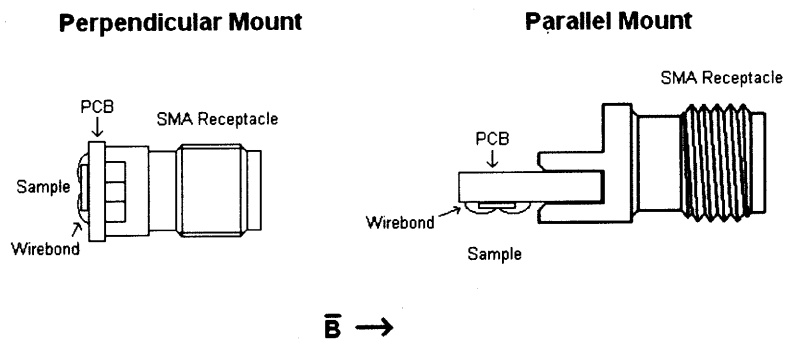

Figure 10: Above are schematics for the two types of probe tips I constructed. None of the materials were ferromagnetic. During the actual experiment, I wrapped this probe in insulator (tape) to prevent any electrical contact with the magnet or dewar manifold.

belly with liquid helium.

It should be noted that the inner probe consisting of the RF coaxial cable and sample mount remain outside the dewar during the cooling process. This is to prevent damage to and contamination of the sample or the wirebonds. Since the inner probe is small and thermally insulating due to its primarily non-magnetic stainless construction, we minimize helium loss due to sample-cooling, allowing for repeated experiments on multiple samples with virtually no experimental overhead.

Once the inner probe is in place, one can begin the experiment. For this work, I performed a large initial sweep of magnetic and current biases. I characterized the dark count rates at each of these conditions by integrating counts over thirty seconds. At this integration time, the count numbers were large enough to prevent significant Poisson error.

After characterizing dark count rates, I began to characterize the photoresponse of the detector at the same range of conditions. I coupled the fiber optic line to a 0.7mW fiber laser source. However, the coupling has unknown attenuation, and the fiber is unfocused towards my detector, so the attenuation rate is unknown. In spite of this, I can still compare relative count rates to characterize relative efficiencies of the detector under different conditions. I began this experiment, but due to the long duration of this experiment, I was unable to maintain the detector at 4.2K long enough to obtain a full range of data points. As such, general trends can be observed,

but only qualitatively.

6.2 Raw Data

The first check of how our detector behaves is to measure the change in critical current with magnetic field strength. This is given in figure 11.

This behaves roughly as expected. Note that although the critical field of NbN is in fact closer to 12T, we are observing a much smaller critical field due to the fact that the film is only 6nm in thickness.

Each point on the above plot represents a data set that I took measuring count rate versus I_b. The outer four points were taken at T=4.2K. These correspond to initial characterizations of dark count rates to be presented later. Since I do not have a temperature probe on the sample, I use these points to measure relative temperature for latter experiments.

In figure 11 (b), I have fit these four points to a second order polynomial. The critical current of NbN has been characterized to have this second order polynomial dependence on H_c.[19]. This predicts a critical field between 2-2.5T, which is quite suppressed. This occurs because our film is very thin. In fact, it is on the order of the penetration depth $\xi \approx 7$nm. Therefore, it is to be expected that our critical field is diminished.

I began to measure the photoresponse of the detector at various applied magnetic field. However, I was only able to collect two data points before the temperature of the sample increased. These data sets are displayed in blue. I continued to measure I_c at various magnetic fields as temperature increased. These data points are shown in red. Notice that I_c is distinctly suppressed. Therefore, even without a calibrated temperature probe, we can measure relative temperature.

First, I characterized the dark count rates of the detector over the total measurable dynamic range of the detector. It is very important to note that I was only able to test up to a magnetic field of approximately 7900 G. This is not due to any physical limitation of the system, rather it is due to the fact that it was at this bias condition that the output voltage pulse became too close to the noise floor to distinguish using my discriminator/counter. There was a measurable (although small) 100MHz pickup. This can be further minimized with additional shielding and/or lower noise RF parts.

Another important factor in determining the minimum pulse size is the discriminator itself. The pulses themselves were not more than 10-20mV high, and as such,

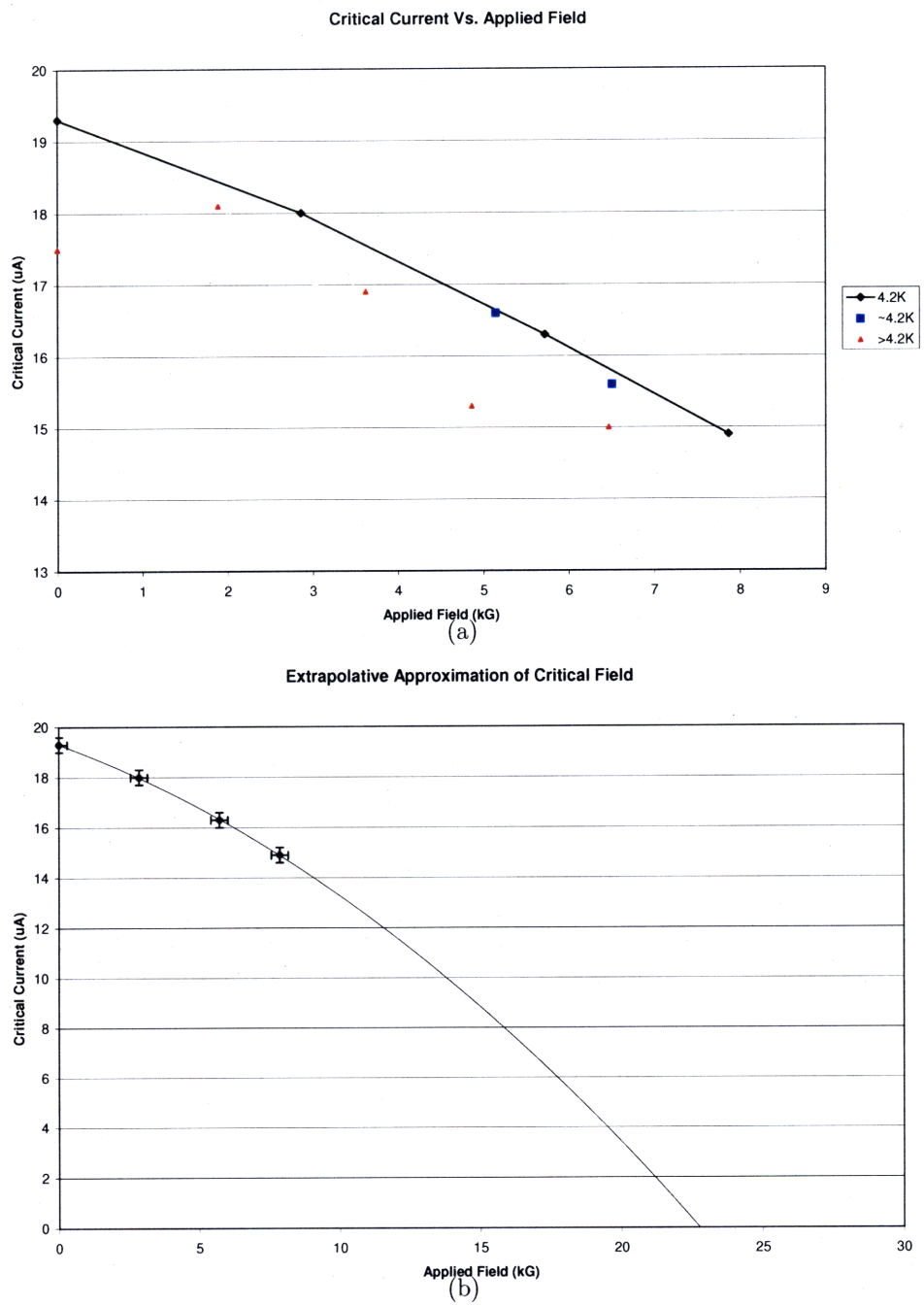

Figure 11: (a) A plot of I_c versus B. The outer curve was taken at 4.2K and each point corresponds to a data set for dark counts. The blue points correspond to a datasets where I characterize the photoresponse. The red points demonstrate data points I took with T>4.2K. One can observe the suppression of I_c. (b) A second order extrapolation of critical current down to 0 uA. This indicates that $H_c \times \mu_0$ is on the order of 2-2.5T

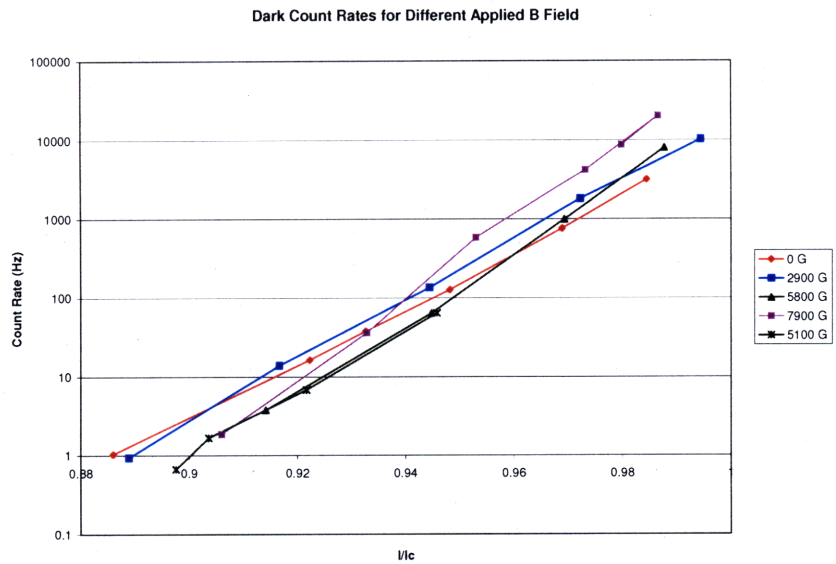

Figure 12: Plot of current-dependent count rates for varying applied magnetic field. First, we observe a definite linear trend as expected. However, note that the slope of each line increases for increasing magnetic field.

I was approaching the sensitivity limit of the discriminator. This can be fixed by adding an additional 10dB amplifier to the chain.

This having been said, I have definitely covered the vast majority of the relevant parameter space. The data is shown in figure 12.

Next, I successfully measured the photoresponse as well as dark count rates for identical photon inputs for two sets of bias conditions, shown in figure 13. Note that this behavior reflects the same type of behavior as the dark count rates. The higher magnetic field has a higher count rate and therefore higher efficiency. At bias conditions farther off of the critical current, the count rates seem to asymptotically approach each other, but I am hesitant to apply any significance to this, as the error associated with these measurements is fairly large, so these smaller features are likely meaningless.

For experimental completeness, I also took some data even when the system was warming up. I noticed for these data runs that there was a massive increase in photon counts and dark counts (thermal phase slips). However, I could not accurately determine temperature and this is not a parameter I wished to vary in my experiment, so I shall ignore these data points henceforth.

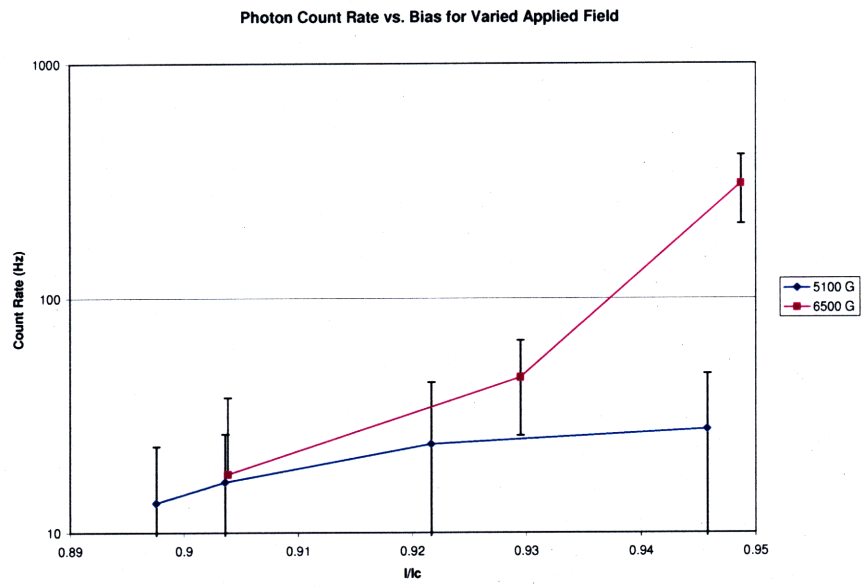

Figure 13: Photon count rates versus bias current for 2 different field conditions. I have subtracted off the baseline dark count rate. There is significant error in these data points, but I am confident that they show a trend of increasing count rates for higher magnetic field.

7 Discussion

7.1 Observed Trends

From figure 12, one can observe that the dark count rates have higher drop-off rates for larger applied magnetic field. Although the structure in the mid-range is convoluted, the limit as current approaches zero and the critical current have a distinct order.

In the limit as current goes to zero, one observes that the dark-count rates for zero applied magnetic field are largest, and the rates decrease monotonically with applied magnetic field.

In the limit as current approaches I_c, one observes that the dark-count rates for zero applied magnetic field are smallest, and the rates increase monotonically with applied magnetic field.

This is a very interesting effect, because if magnetic field biasing were a purely linear effect, one would expect these dark count rates to be approximately the same regardless of the applied field. Instead, we see approximately an order of magnitude difference between the dark count rates of zero magnetic field bias and 7900 G magnetic field bias near the critical current.

It is also important to note that I swept magnetic field from zero to 7900 G for this measurement and then took data when decreasing the field and testing the photoresponse. The dark count rates from the 5100 G measurement are shown. Note that it matches very well with the observed trends and tracks the 5800 G trendline. This excludes the possibility of any system drift or time dependence and helps demonstrate the relative accuracy of our points.

When sweeping the magnetic field down, I also measured the photoresponse of the detector. Qualitatively, they behave much in the same way as the dark counts, which is to be expected, if we believe that dark counts and detection efficiency are related to ΔF_0.[17]

There also appears to be an asymptotic behavior as bias current approaches zero, but this may be due to the large error margins at lower photon count rates. Really all we can conclude from this data is that an increase in magnetic field qualitatively increases the photoresponse of a detector. Beyond this, we have too much uncharacterized error to make significant claims.

In conclusion, we have found that an applied magnetic field increases the dropoff rate of dark counts, while increasing the observed counts at high bias currents.

For photoresponse we have found that an applied field increases the sensitivity of the detector for identical I/I_c ratios.

7.2 Sources of Error

It should be noted that I have not included error estimates on most of the plots in the above two sections. This is primarily due to the fact that any error would be an order-of-magnitude estimate. I simply do not have enough data to put a precise value on the errors for each point. However, I do have a good enough understanding of the errors to give a reasonable estimate which proves the validity of my data.

The largest source of systematic error is due to the lack of characterization of the magnetic field within the superconducting magnet. Not only are we assuming complete linearity with the magnet specification, we are also ignoring the earth's magnetic field and the fact that there is a superconducting ring around the entire detector which will screen some of the field. Therefore, we can only claim accuracy down to $\sim$100 G.

Since we are unsure as to exactly how magnetic field affects the count rate of the system, it is difficult to determine exactly how this error should propagate to the observed output. The only method of doing this is to perform this experiment again

with finer granularity, so that we may plot count rates versus applied magnetic field and take the derivative.

More importantly, this is a purely systematic offset. This error does not affect any of the trends in dark count rates observed in the previous sections. For the initial claims regarding data trends that I am trying to make with this data, this error makes no significant impact.

Another source of error in this experiment is due to the counting strategy. First, we are only counting for a finite time, so technically we have a non-zero Poisson error, but these errors are largely insignificant due to the high count rates and large integration times.

More importantly, the pulses produced by the photon detector were very small (20-40mV after amplification), so the signal to noise ratio for some cases was no more than 5-10. The error comes with the fact that this interval is pushing the sensitivity limit of our discriminator/counter. Therefore, in some cases, it is likely that the counter included some noise pulses as signals.

However, I recalibrated the discriminator for each data set to minimize the number of false counts. In addition, any background noise is constant, so this would be observed as a constant offset for a given data set. For each data set, I observed count rates on the order of 1 Hz, so any baseline noise counts would have to be below this. The trends I am observing are on the order of 100-1000 Hz, so this error does not overwhelm my observation.

Also, there is some error in the measurement of I_c and the bias current. Our current source is slightly nonlinear, so the current readout varies from the actual sourced current. However, this deviation is not more than $\sim 0.3\mu$A.

One of the largest and most worrying potential sources of uncalibrated error was due to the temperature fluctuations of the sample near the end of the experiment. This definitely affected observed count rates significantly (an order of magnitude difference).

To ensure that this fluctuation did not affect our data, I looked for suppressed critical current at identical bias conditions as I had measured previously in the evening. These affected data sets are demonstrated by the red points in figure 11.

First, I am confident that temperature had minimal impact on the photoresponse data due to the lack of suppression of critical current. One additional source of confirmation of the lack of temperature change in the photoresponse measurements is that I simultaneously characterized dark count rates. These count rates matched

those taken in the previous run and followed the same trends. The dark counts measured at 5100 G during my test of the photoresponse match especially closely to the 5800 G trend. This is explicitly shown in figure 12. This is encouraging to confirm lack of noise in the photoresponse data because the dark count data sets and the photoresponse data sets were taken at significantly different times and in different orders.

Dark count rates of the 6500 G measurement are slightly larger by a constant multiplicative factor; likely due to a slight temperature change. To compensate for this, I have not only subtracted off the dark counts from the photoresponse, I have included this percentage error as the error margin for each of these points. Even with this larger error margin, the increase in detection efficiency is readily shown in figure 13.

7.3 Continuation of Experiment

Now that this experiment has been constructed and tested, it is time to go back and take a much finer set of data with a larger degree of repetition. This will allow us to quantitatively characterize the trends I have only observed qualitatively up to this point. With these data, it should be much more feasible to come up with a theoretical explanation for the new behavior observed.

In addition, I mentioned previously that I have an additional probe with the sample mounted parallel to the field instead of perpendicular. I will preform this experiment with the sample mounted in this orientation to observe how the angle of the magnetic field affects the detector's behavior.

Finally, it may be worthwhile to change the fabrication template. Currently, there is a ring of superconductor surrounding the detector. This acts to partially shield the detector from magnetic field. If we remove this ring, it will be easier to understand exactly how the detector is responding to specific magnitudes of magnetic field.

7.4 Potential Extensions

This experimental work demonstrates that it is possible to detect photons with magnetic field biasing. Currently we are still using a voltage readout from a nonzero bias current, but it should theoretically be possible to use other options. For example, we could use an entirely magnetic system with a SQUID readout instead of an RF voltage readout.

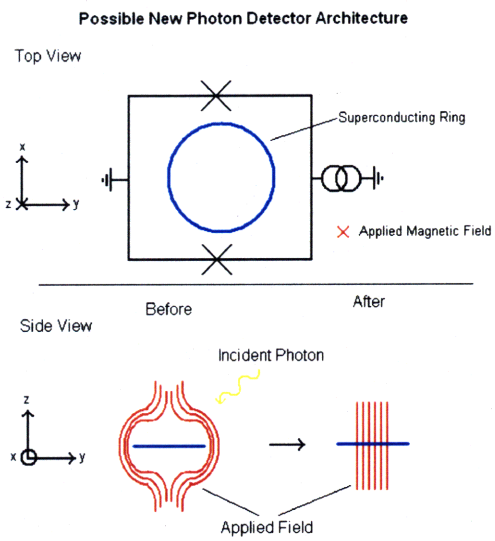

Figure 14: A schematic of proposed detector architecture. A single superconducting ring inside of a SQUID. In an applied B field, if an incident photon causes the ring to become normal, one should be able to read this out on a the SQUID.

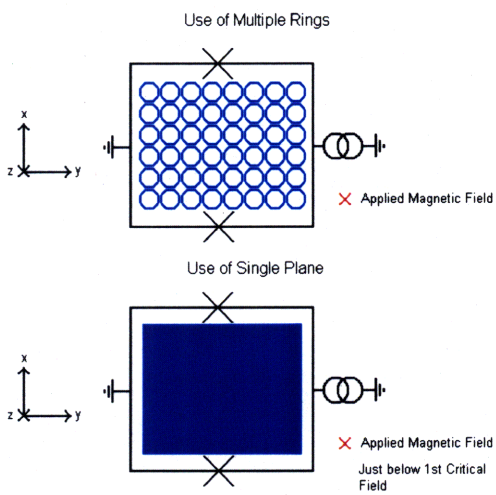

Figure 15: Generalizations of the architecture in figure 14. One simply has multiple rings. The other idea is to use vortices for detection purposes. However, optical formation of vortex-antivortex pairing in the presence of magnetic field is not very well understood, and merits further investigation.

Consider a loop of superconducting wire that encloses a SQUID as in figure 14. Now, if we choose the superconductors such that the critical field of the loop of wire is significantly less than that of the superconductor composing the SQUID, we can set up a constant bias magnetic field around this entire system.

If we choose the magnetic field such that is just below the critical field of the outer superconducting ring, this ring will prevent magnetic field from the SQUID until an incoming excitation, such as a photon breaks the superconductivity. Now, all of the excluded magnetic field can try to enter the SQUID, which can be read on the SQUID output.

Note that for fabrication, we must choose a geometry where it is difficult for a fluxon to escape the superconducting ring without affecting the flux through the SQUID. This should be possible if the ring and SQUID are in the same plane and there is not significant space between the two.

With this setup, one can detect a single photon before manually resetting the system. Once the ring goes normal, it allows magnetic field into the system. When the system returns to superconducting state, this field is locked in. Therefore, one must completely remove the B field and cycle the conductive states before we can detect another photon. This is completely unreasonable.

Now, consider if we had multiple loops of superconducting wire within the SQUID ring as in figure 15. If each wire is isolated from each other, then we can consider the switching mechanism of each of these rings independently.

Once again, we bias the system to just below the critical field. Now, any incident photon would cause a small section of the superconductor to go normal for a short period of time. Now, we must consider the minimum possible size of these rings. A SQUID can detect a single fluxon of magnetic field: $2.07 * 10^{-15} W$. Now, we have to operate at a reasonable magnetic field strength: between 1-10T (H_c of NbN is 12T, but this is suppressed for thinner films). To detect the switching of a single ring, the flux through this ring must be about equal to a single fluxon. This reveals that a single ring must enclose $\approx$1000nm^2.

First, we recognize that this area is significantly larger than the hotspot of a normal incident photon. Therefore, even though the area of a hotspot should scale with the energy of the incoming photon, we will not be able to detect different energy photons (until the hotspot area is greater than 1000 nm^2: which would only occur with extremely high energy photons).

We still haven't solved the reset problem once a ring goes normal, we can't reuse

it until we reset the system. However, we are interested in larger active areas for the purposes of photon detection. As we make this system large, the number of counts grows quadratically with area. For a $1mm^2$ active area with a $1000nm^2$ ring size, one can count 10^9 photons total, or approximately 10^8 before your detection efficiency changes significantly. Now, it takes a much longer time for the detector to saturate, so it does not need to be reset nearly as often.

In addition, this approach should dramatically reduce switching time, as the thermal and electrical time constants are lower. The kinetic inductance is not nearly as significant, as we are not depending on meanders. Also, there is no joule heating due to bias current, so the reset time is limited only by the energy of the photon and the thermal resistance of the system.

Although the functionality of the above two architectures is fairly straightforward, one may consider the possibility of biasing a solid type-2 superconductor just below its first critical field (see figure 15). In this case, an incoming photon could transfer enough energy to form a vortex to be detected by the SQUID. However, very limited study has been executed in the formation of vortices by photons in a high-magnetic field environment, so there is no direct empirical evidence to demonstrate the feasibility of this final architecture.

8 Conclusion

In conclusion, I have investigated the behavior of NbN nanowires as their widths approach the coherence length. In this regard, I have established a working lower bound for the width of wires before the wire becomes too resistive to be of use for photon detection. Specifically, operating at 4.2K, the minimum wire width appears to be between 20-30nm depending on what dark count rate you can tolerate for your specific application.

Secondly, I have constructed an experimental apparatus capable of investigating the SNSPDs with magnetic field biasing. I have taken initial data on this front that indicates that these bias conditions increase detection efficiency. However, the initial data is only enough to make qualitative judgements. A more careful pass must be taken before we can make any quantitative conclusions.

In addition, this experimental platform was constructed with a more general purpose. I specifically tested photon detection under magnetic field. However, the cryostat, probes, and supplies can all be used for more general purpose magnetic field

experiments. One specific application of this is to better characterize the superconductors grown locally. Currently, we can only measure a few parameters with a R/T curve. However, if we can sweep magnetic field as well, we can calculate a great deal more.

Finally, after demonstrating the possibility of detecting photons using magnetic field biasing, I have proposed a possible new photon detector architecture using only magnetic field biasing and SQUIDs as a readout. This new architecture is very feasible and seems to have certain advantages over the current architecture.

9 Acknowledgments

I would like to thank Prof. Karl K. Berggren for providing me the opportunity to fulfill this project as well as for many helpful discussions regarding problems I encountered over the course of this experiment.

I would like to thank Dr. Eric Dauler for fabricating all of my samples as well as helping me with debugging noise problems with my RF setup.

I would like to thank Xiaolong Hu for lending me the RF setup and helping me debug noise problems.

I would like to thank Prof. Rajeev Ram for lending me his parameter analyzer to perform the ultranarrow nanowire experiment.

I would like to thank Prof. Carver Mead from the California Institute of Technology for donating the superconducting magnet for my experimental setup.

I would like to thank Yunjie Ma for designing the low-noise current source used to bias the photon detector.

References

[1] M. A. Jaspan, J. L. Habif, R. H. Hadfield, and S. W. Nam, "Heralding of telecommunication photon pairs with a superconducting single photon detector," *Appl. Phys. Lett*, vol. 89 (2006)

[2] H. Takesue, S. W. Nam, Q. Zhang, R. H. Hadfield, T. Honio, K. Tamaki, and Y. Yamamoto, "Quantum key distribution over a 40-dB channel loss using superconducting single-photon detectors," *Nature Photonics* vol. 1, pp. 343-348, 2007.

[3] K. M. Rosfjord, J. K. W. Yang, E. A. Dauler, A. J. Kerman, V. Anant, B. M. Voronov, G. N. Gol'tsman, K. K. Berggren, "Nanowire Single-photon detector with an integrated optical cavity and anti-reflection coating," Opt. Express 14, 527 (2006)

[4] J. Bardeen, L. N. Cooper, and J. R. Schrieffer, "Theory of Superconductivity." Phys. Rev. 108, 1175 (1957).

[5] A. J. Kerman et al., "Constriction-limited detection efficiency of superconducting nanowire single-photon detectors." Appl. Phys. Lett. 90 (2007)

[6] A. Engel, A. Semenov, H. W. Hubers, K. Ilin, M. Siegel, "Dark counts of a superconducting single-photon detector." NIMA 520 32-35 (2004)

[7] C. N. Lau, N. Markovick, M. Bockrath, A. Bezryadin, and M. Tinkham, "Quantum Phase Slips in Superconducting Nanowires," *Phys. Rev. Lett.*, vol. 87, no. 21, (2001)

[8] A. T. Bollinger, R. C. Dinsmore III, A. Rogachev, A. Bezryadin, "Phase Diagram of the Superconductor-Insulator Transition in One-Dimensional Wires," *Phys. Rev. Lett.*, Vol. 101, 22 (2008)

[9] N. Giordano, "Dissipation in a one-dimensional superconductor: Evidence for macroscopic quantum tunnelling," *Phys. Rev. B*, Vol. 41, no. 10, pp. 6350-6365, (1990)

[10] J. K. W. Yang, K. K. Berggren, "Using high-contrast salty development of hydrogen silsesquioxane for sub-10-nm half-pitch lithography," *J. Vac. Sci. B*, 25, 2013 (2007)

[11] D. E. McCumber and B. I. Halperin, "Time scale of intrinsic resistive fluctuations in thin superconducting wires," *Phys. Rev. B*, vol. 1, pp. 1054-1070, 1970.

[12] A. Verevkin, J. Zhang, R. Sobolewski et al., "Detection efficiency of large-active-area NbN single-photon superconducting detectors in the ultraviolet to near-infrared range." Appl. Phys. Lett 80, 25 4687 (2002)

[13] J. K. W. Yang, A. J. Kerman, E. A. Dauler, V. Anant, K. M. Rosfjord, K. K. Berggren, "Modeling the Electrical and Thermal Response of Superconducting

Nanowire Single-Photon Detectors." IEEE Trans. Appl. Supercond. 17 (2) pp. 581-585 (2007)

[14] A. J. Kermen, J. K. W. Yang, R. J. Molnar, E. A. Dauler, K. K. Berggren, "Electrothermal feedback in superconducting nanowire single-photon detectors," *Phys. Rev. B*, 79, 100509 (2009)

[15] A. D. Semenov, G. N. Gol'tsman, "Hot-electron effect in superconductors and its applications for radiation sensors." Supercond. Sci. Technol. 15 (2002) R1-R16

[16] A. J. Kerman, E. A. Dauler, W. E. Keicher, J. K. W. Yang, K. K. Berggren, G. Gol'tsman, B. Voronov, "Kinetic-inductance-limited reset time of superconducting nanowire photon counters." Appl. Phys. Lett. 88, 111116 (2006)

[17] J. Kitaygorsky et al., "Origin of Dark Counts in Nanostructured NbN Single-Photon Detectors." IEEE Trans. Appl. Supercond. 15 (2) pp. 545-548 (2005)

[18] A. Semenov, A. Engel, K. Il'in, G. Gol'tsman, M. Siegel, H. W. Hubers, "Ultimate performance of a superconducting quantum detector." Eur. Phys. J. AP 21. 171-178 (2003)

[19] D. P. Hampsire, K. E. Gray, R. T. Kampwirth, "Scaling laws for the critical current density of NbN fils in high magnetic fields." IEEE Trans. Appl. Supercond. 3 1 4 pp. 1246-1252 (1993)